Science Advances

AAAS

advances.sciencemag.org/cgi/content/full/4/2/eaao6724/DC1

Supplementary Materials for

Liquid gating elastomeric porous system with dynamically controllable gas/liquid transport

Zhizhi Sheng, Honglong Wang, Yongliang Tang, Miao Wang, Lizhi Huang, Lingli Min, Haiqiang Meng, Songyue Chen, Lei Jiang, Xu Hou

Published 9 February 2018, *Sci. Adv.* **4**, eaao6724 (2018)
DOI: 10.1126/sciadv.aao6724

The PDF file includes:

- fig. S11. Critical pressure of water passing through different gating liquids in two types of membrane materials.
- fig. S12. The pressure of gas and liquid after cycles of stretch and relaxation.
- fig. S13. Images of nonstretched and stretched EPMs.
- fig. S14. Different pore size distribution leads to different gating performance.
- Legends for movies S1 to S4

Other Supplementary Material for this manuscript includes the following:
(available at advances.sciencemag.org/cgi/content/full/4/2/eaao6724/DC1)

- movie S1 (.mp4 format). Preparation and mechanism of LGEPM system.
- movie S2 (.mp4 format). One-dimensional stretching of EPM.
- movie S3 (.mp4 format). Dynamic deformation of LGEPM.
- movie S4 (.mp4 format). Dynamic gas and liquid separation process by LGEPM.

Supplementary Materials

section S1. Multiple methods to fabricate porous membranes with various pore sizes on different EMs

In the main text, we mention that the elastomeric porous membrane could be fabricated by CO_2 laser cutting, femtosecond laser cutting and Si replica molding method. These three methods can be used to fabricated the pores from 5 μm to 350 μm. Specifically, the pores ranging from 50 μm to 350 μm can be obtained by CO_2 laser cutting. Those ranging from 5 μm to 20 μm can be obtained by femtosecond laser cutting and those ranging from 5 μm to 200 μm can be obtained by Si replica molding method.

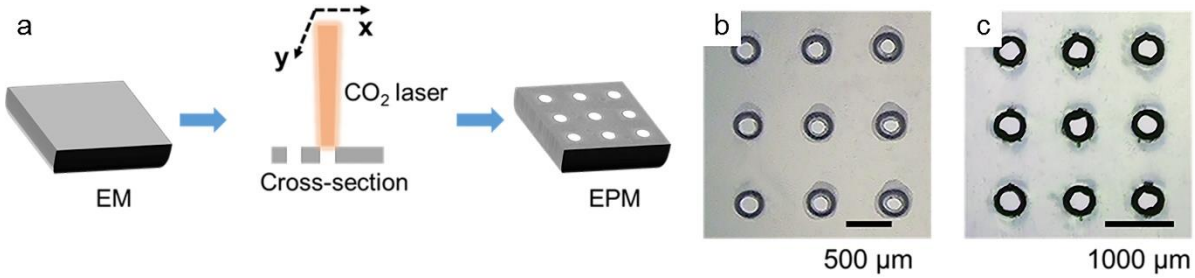

fig. S1. The fabrication of EPM by CO_2 laser cutting and its morphology. (**a**) Fabrication process of EPM by CO_2 laser cutting. (**b** and **c**) Microscopic image of EPM with pore size of 200 μm (b) and 340 μm (c). Scale bar, 500 μm in (b) and 1000 μm in (c).

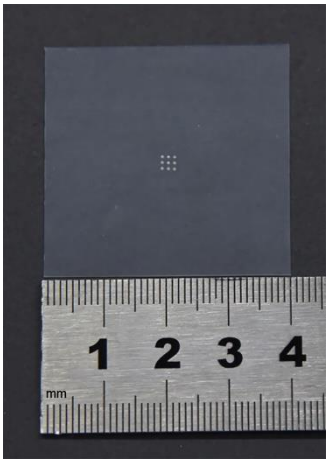

fig. S2. The image of a whole silicone rubber membrane with nine pores in the center.

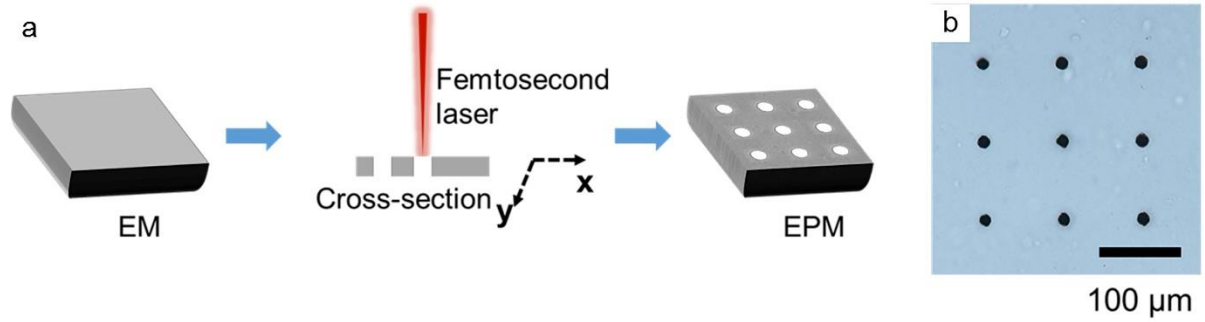

fig. S3. The fabrication of EPM by femtosecond laser cutting and its morphology. (**a**) Fabrication process of EPM by Femtosecond laser cutting. (**b**) Microscopic image of EPM with pore size of 15 μm. Scale bar, 100 μm.

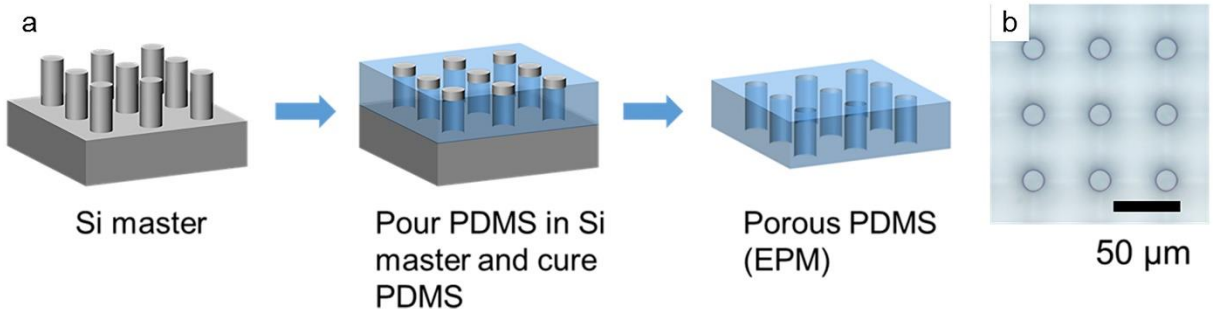

fig. S4. The fabrication of porous PDMS membrane by Si replica molding method and its morphology. (**a**) Fabrication process of porous PDMS membrane. (**b**) Microscopic image of a porous PDMS membrane the pore size of 16 μm. Scale bar, 50 μm.

section S2. The theoretical model agrees with the experimental critical pressure at a series of flow rates

We theoretically fit the experimetal data of water transport through the LGEPM (using equation (3) and (4)), obtaining the material parameters Φ=0.029 and σ=1.5 μm. Then, we study the perfomance of the system with various pore sizes in Fig.4A.

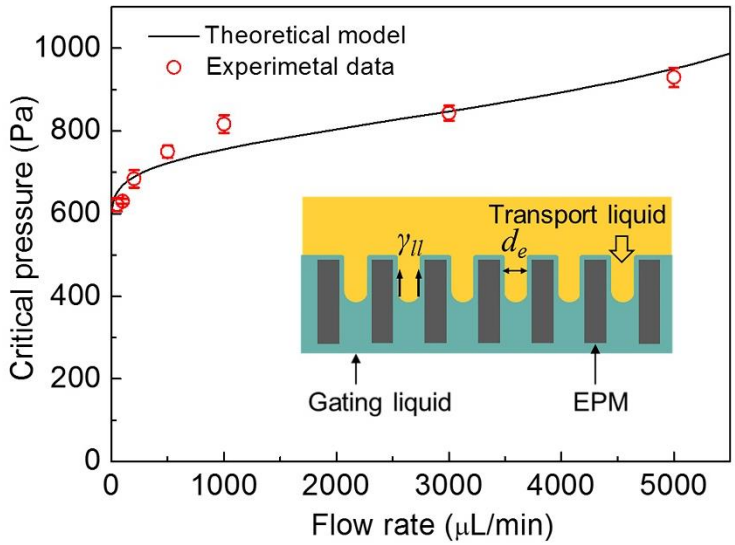

fig. S5. The experimental and theoretical models of critical pressure of water transporting through the LGEPM at different flow rates. The inset indicates the schematic model to determine the critcial pressure of liquid. The gating pressure is related to the pore size and the liquid-liquid interfacial surface tension.

section S3. Deformation of EPM under one- or two-dimensional stretch

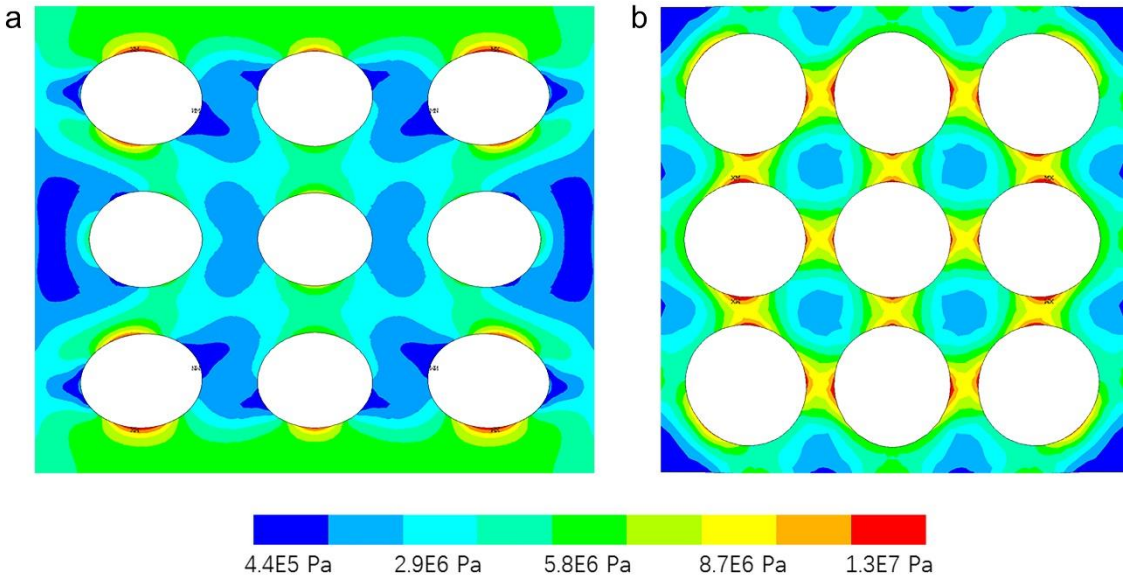

fig. S6. Stress distribution of the elastomeric multiporous membrane. (a) The stress distribution of a 3×3 array of pores with one-dimensional stretch. (b) The stress distribution of a 3×3 array of pores with two-dimensional stretch.

section S4. Critical pressure change in various LGEPM systems.

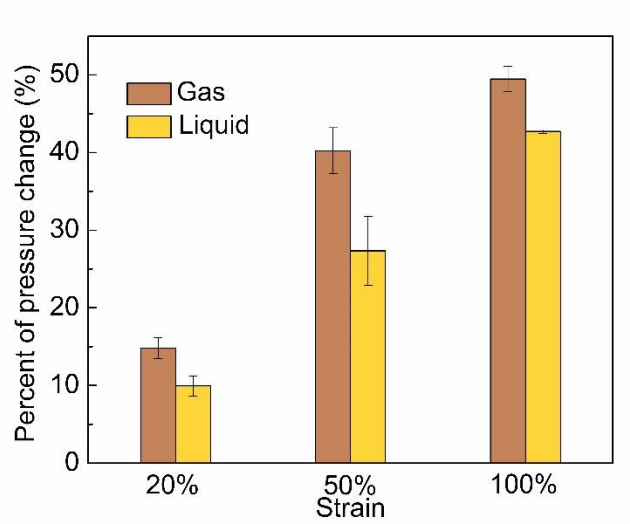

fig. S7. Different pressure change via different deformation extent.

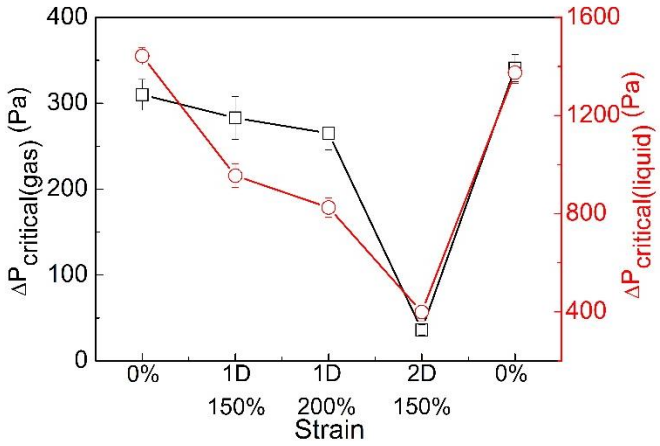

fig. S8. Critical pressure change of bare silicone rubber membranes in a static stretching process. Pore size is 150 μm.

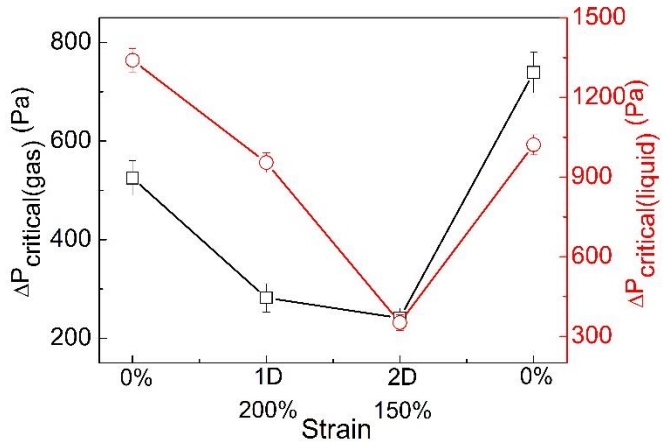

fig. S9. Critical pressure change of silicone oil–infused silicone rubber membranes in a static stretching process. Pore size is 150 μm.

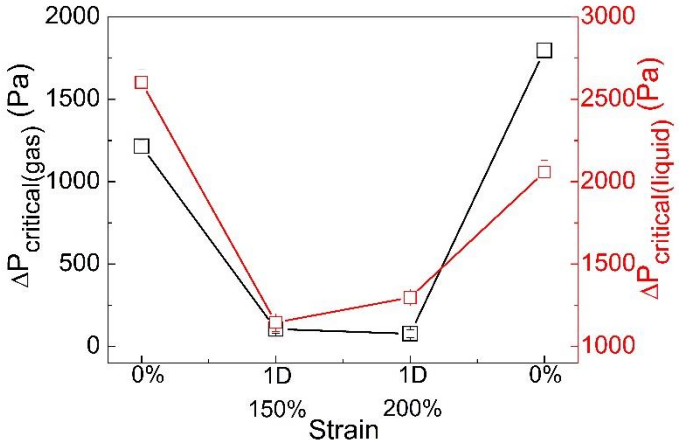

fig. S10. Critical pressure change of liquid paraffin–infused silicone rubber membranes in a static stretching process. Pore size is 150 μm.

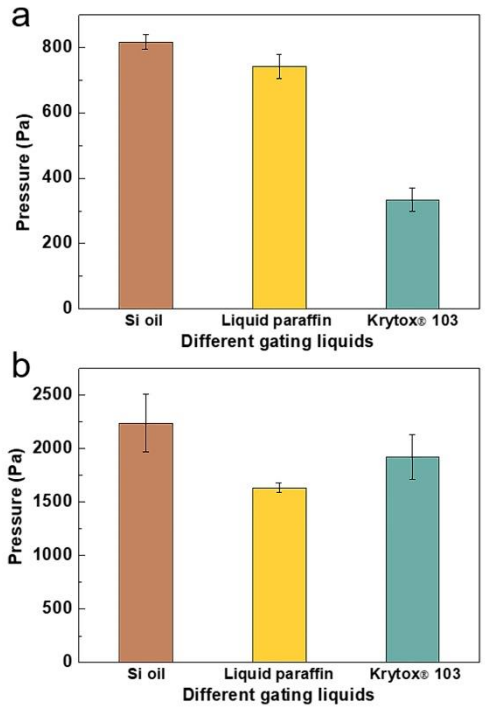

fig. S11. Critical pressure of water passing through different gating liquids in two types of membrane materials. (**a**) The same silicone rubber porous membrane with different gating liquids. (**b**) The same PDMS porous membrane with different gating liquids.

section S5. Durability of the LGEPM system

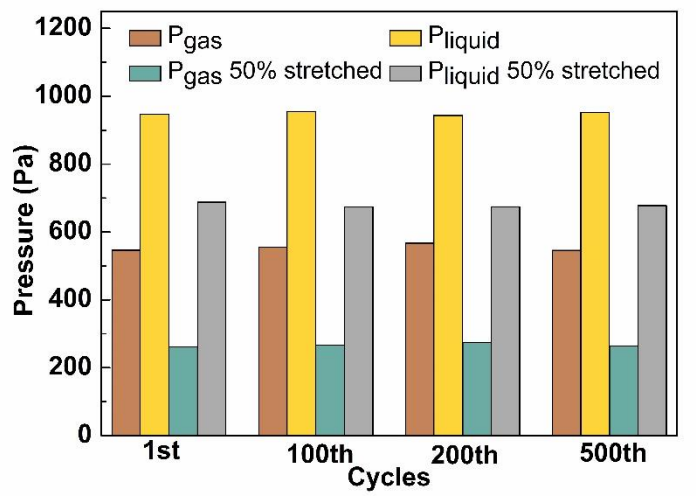

fig. S12. The pressure of gas and liquid after cycles of stretch and relaxation. Pore size is 200 μm.

section S6. Uniformity of the EPMs during deformation

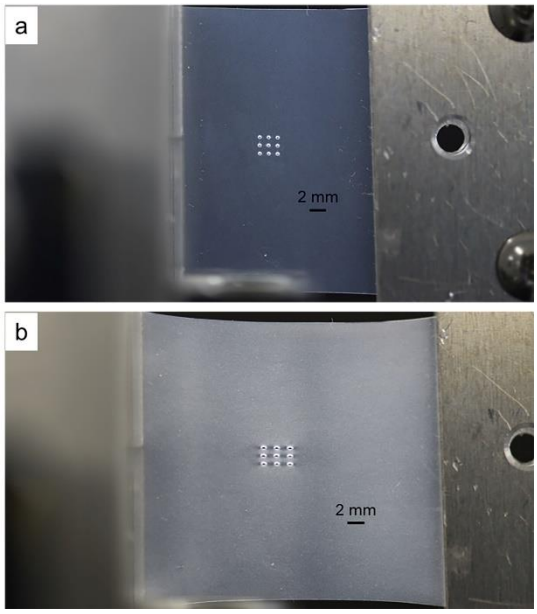

fig. S13. Images of nonstretched and stretched EPMs. (**a**) A non-stretched elastomeric porous membrane. (**b**) A stretched elastomeric porous membrane. The porous membrane is silicone rubber.

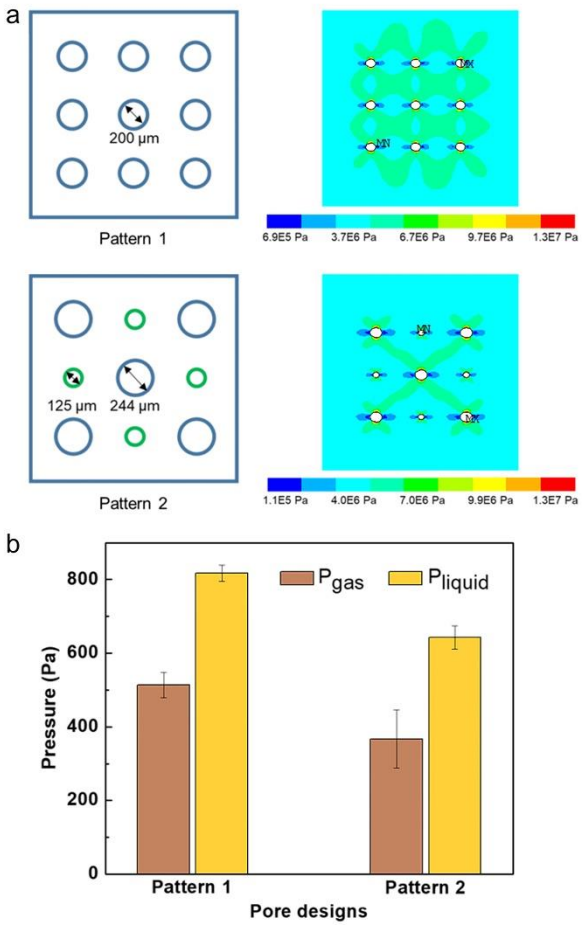

fig. S14. Different pore size distribution leads to different gating performance. (**a**) The same pore area with different pore size distributions and their strain distributions. (**b**) The corresponding gating behavior of the two different pore designs.

Supplementary movies

movie S1. Preparation and mechanism of LGEPM system.
movie S2. One-dimensional stretching of EPM.
movie S3. Dynamic deformation of LGEPM.
movie S4. Dynamic gas and liquid separation process by LGEPM.